Influence of curing-induced pre-deformations on the mechanical properties of adhesively bonded joints in steel-intensive mixed-material structures

F. Beule[1], D. Teutenberg[1], G. Meschut[1], T. Aubel[2], A. Matzenmiller[2]

[1]Paderborn University, Laboratory for Material and Joining Technology (LWF), Pohlweg 47-49, 33098 Paderborn, Germany

[2]University of Kassel, Institute of Mechanics (IfM), Mönchebergstraße 7, 34125 Kassel, Germany

Summary

Due to modern multi-material design, the curing of thermosetting adhesives is accompanied by relative displacements of the joining partners. This leads to highly complex thermo-chemo-mechanical stress-states within the adhesive layer. In this study, experiments are conducted to examine the influence of process-related thermal relative displacements on the mechanical properties of adhesives. The results show an anisotropy of the mechanical properties of the pre-deformed adhesive layers, depending on the magnitude and direction of the relative displacement. Further, the findings are implemented into the consisting Toughened Adhesive Polymer (TAPO) model to be used for numerical simulations with LS-DYNA.

Keywords

Adhesive Bonding, Epoxy Structural Adhesive, Relative Displacements, Influence of Manufacture, Numerical Simulation, Multi-Material Design, Kinematic hardening, Isotropic hardening, Cure dependency, Temperature dependency

Introduction

The ongoing introduction of multi-material design into modern lightweight construction places new demands on the joining technology of hybrid structures [1]. Adhesive bonding technology is particularly used for highly stressed and safety-relevant components made of different materials. The adhesive joints generally have a major influence on the characteristics of the relevant operating properties. They are decisive for the stiffness, fatigue strength and crash properties. Particularly when using thermosetting adhesive systems, based on epoxy resins in hybrid components with varying thermal expansion coefficients, however, the joints are already subjected to stress during the curing process and in the subsequent cooling phase [2]. This can significantly influence the properties of the cured adhesive bond. In terms of a computational design, the influence of thermally induced displacements is of interest during the manufacturing process on the load-bearing capacity in operational load cases and it is not considered in current investigations.

The aim of this study is to develop a holistic method for failure analysis, considering relative displacements of the joining partners during the curing process. Basic tests are carried out in order to investigate the influence of these relative displacements at hand. The specimens are cured with different temperature-displacement-time profiles and subsequently tested quasi-statically. The test results used for the parameter identification of the extended TAPO model to include pre-damage, based on thermally induced load changes in the manufacturing process.

Methodology

The basic tests are carried out by using thick adherend shear specimens (TASS) and butt joint specimens (BJS) in accordance with the DIN EN 14869-2 [3] and DIN EN 15870 [4]. As adhesive, DuPont Betamate 1496V is selected which is a one-component, thermosetting, toughened adhesive based on epoxy resin. Curing takes place in a universal tensile-compression testing machine with an integrated temperature control circuit. This allows the specimens to be heated and cooled in a targeted manner while they are being displaced relative to each other. Thus, it is possible to apply defined temperature-displacement-time profiles and to introduce specific pre-deformation into the adhesive layer.

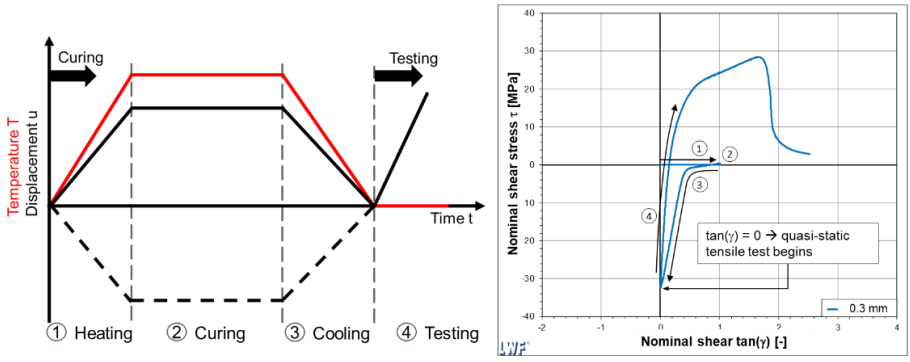

Figure 1. Temperature-displacement-time profile (left) and representative shear stress-shear diagram (right) for the continuous curing and testing process for the TASS.

For curing idealised temperature-displacement-time profiles are defined, based on the cathodic dip-drying process. Figure 1 shows an example for the TASS. First, there is the heating phase (1), whereby the specimens are heated at 10 K/min. Using temperature-compensated clip-on strain gauges, the specimens are moved from the initial state to a defined relative displacement. Subsequently, the curing phase (2) has a duration of 30 min at 180 °C under a constant displacement value. The cooling phase (3) follows as the joining partners are being moved to their initial position whilst being cooled down at 10 K/min to room temperature. Next the quasi-static test phase (4) with a testing speed of v = 0.036 mm/min, corresponding to a nominal initial principal strain rate of $\dot{\gamma} = 0.01\ s^{-1}$, follows the joining process. All tests form the basis for numerical material modelling, in which the processes of curing and testing are considered together as a single process. The plot on the right in Figure 1 shows an example of a shear stress–shear diagram, obtained from the continuous process. To investigate the directional dependence of the mechanical properties due to thermally induced pre-deformation, additional specimens are pre-deformed in the

opposite, negatively defined direction (dashed line). In contrast to the TASS, the BJS are unloaded to a force value of 0 N during cooling because returning to the initial position would cause unrealistically high forces.

Experimental Results

Figure 2 shows the shear stress-shear diagrams for the continuous curing and testing process of the TASS with positively defined pre-deformations (left) and negatively defined pre-deformations (right). Based on the results, it becomes apparent that both the magnitude and the direction of the pre-deformation have an influence on the properties of the bonded joint. With increasing pre-deformation in a positively defined direction, both the maximum stress and the yield stress decrease, while the plastic deformation increases. However, if the specimen is pre-deformed in the negatively defined direction, the opposite effects may be detected.

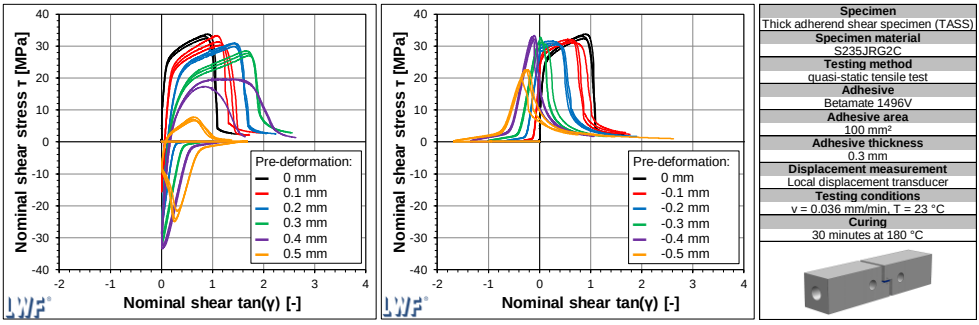

Figure 2. Shear stress-shear diagrams of the continuous curing and testing process of the TASS with positively defined pre-deformations (left) and negatively defined pre-deformations (right).

Additionally, tests are performed on the BJS to investigate the influence in the normal direction of thermally induced pre-deformations on the adhesive layer properties under shear loading. During curing, a reduction in the adhesive area occurs due to the nature of the relative displacement. Therefore, all the tensile stresses, shown in

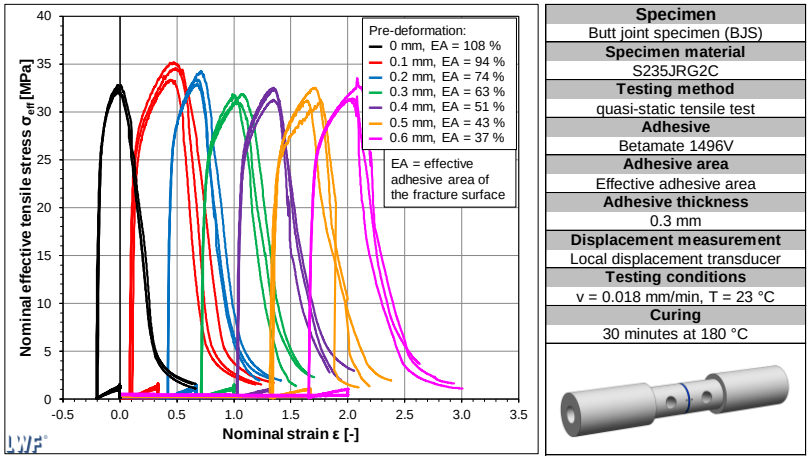

Figure 3. Tensile stress-strain diagram of the continuous curing and testing process of the TASS with pre-deformations.

Figure 3, are related to the effective adhesive area in the fracture cross-section. The individual curves are highly similar. All specimens have the same maximum tensile stress. A stronger plastic phase, however, becomes apparent with an increase in pre-deformation. The pre-deformation of the adhesive layer in the normal direction has less influence on the properties than the pre-deformation in the shear plane.

Numerical modelling

To describe the relationships determined by the experiments, the Toughened Adhesive Polymer (TAPO) [5] model, available in LS-DYNA as *MAT_252 and in an extended version as *MAT_307 (in development), was extended to include the phenomenon of temperature- and state of cure dependent kinematic hardening. It is a cohesive zone model consisting of three components, each in tangential, binormal and normal direction, see figure 4. The displacement jumps Δ and the tractions t are described in eq. (1) and (2).

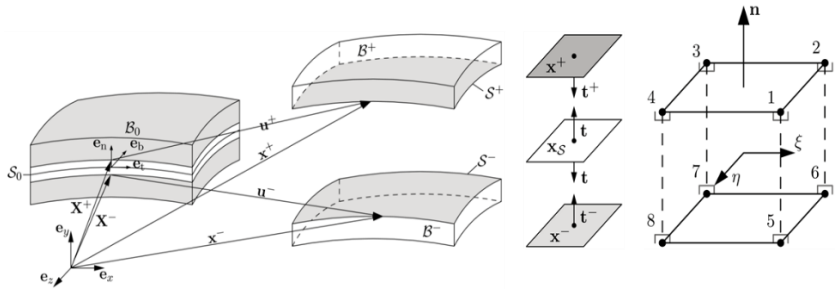

Figure 4: Adhesive layer as an interface approximation in the form of an 8-noded cohesive zone element according to [6].

$$\mathbf{\Delta} = \begin{Bmatrix} \Delta_n & \Delta_t & \Delta_b \end{Bmatrix}^T \tag{1}$$

$$\mathbf{t} = \begin{Bmatrix} t_n & t_t & t_b \end{Bmatrix}^T \tag{2}$$

The rheological network is shown in Figure 5. It consists of a viscoelastic submodel in form of a generalized MAXWELL type model connected in series with the strain hardening model. It is composed of a linear-isotropic hardening part and a nonlinear-kinematic one, which are arranged in parallel combining a friction element representing the yield point. In addition, thermal expansion as well as chemical volume shrinkage due to curing are considered by the expansion element. The calculation of the state of cure as a result of the temperature-time history is based on an extended KAMAL model [7], shown in eq. (3).

$$\frac{dp}{dt} = [K_1(\theta)p^a + K_2(\theta)] \cdot (1-p)^n \tag{3}$$

The stresses of the components of the cohesive zone model are calculated as a viscoelastic history function by integrating the relaxation functions in eq. (4), as described in [8], [9] and [10].

$$\begin{bmatrix} t_n \\ t_t \\ t_b \end{bmatrix} = \int_0^t \begin{bmatrix} R_n(t-\tau) & 0 & 0 \\ 0 & R_s(t-\tau) & 0 \\ 0 & 0 & R_s(t-\tau) \end{bmatrix} \begin{bmatrix} \Delta_n' \\ \Delta_t' \\ \Delta_b' \end{bmatrix} \mathrm{d}\tau \quad \text{mit} \quad \Delta' = \frac{\mathrm{d}\Delta}{\mathrm{d}\tau} \tag{4}$$

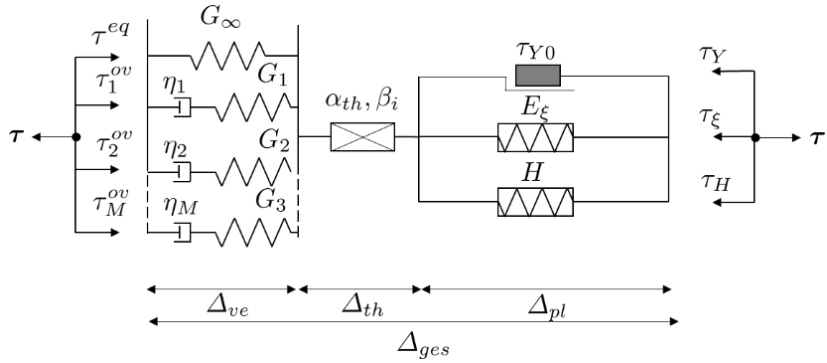

Figure 5: Rheological network of the extended viscoelastic-viscoplastic, temperature- and state of cure dependent TAPO model for the interface involving kinematic hardening

The relaxation functions include the characteristic relaxation time constants $\hat{\tau}_i$, the equilibrium stiffness $\hat{\nu}_\infty$, and the material time $\xi = t/a_{\theta p}(\theta, p)$, which combines the changes in temperature θ and degree of cure p in the form of a horizontal shift function $a_{\theta p}$ of the relaxation spectra taking into account the thermo-chemo-rheological simplicity, see eq. (5) and (6)

$$R_n = k\left[\hat{\nu}_\infty^n + \sum_{i=1}^{M} \nu_i^n \exp\left(-\frac{\xi}{\hat{\tau}_i^n}\right)\right] \tag{5}$$

$$R_s = g\left[\hat{\nu}_\infty^s + \sum_{i=1}^{M} \nu_i^s \exp\left(-\frac{\xi}{\hat{\tau}_i^s}\right)\right] \tag{6}$$

The plastic model follows a non-associated flow rule, which means that the plastic potential $\tilde{f}^*$ and the yield function f are not equivalent:

$$\tilde{f}^* \neq f \tag{7}$$

The yield function itself follows an effective damaged formulation as a function of normal and shear stresses and describes an ellipse that is similar to the DRUCKER-PRAGER criterion for compressive normal stresses.

$$\tilde{f}(\hat{\tau}_n, \hat{\tau}) = \hat{\tau}_\xi^2 + \tilde{a}_1 \tau_{Y0}(\hat{t}_n - t_{\xi n}) + \tilde{a}_2 \langle \hat{t}_n - t_{\xi n} \rangle - \tau_y^2 \tag{8}$$

The plastic potential is obtained by neglecting the linear term:

$$\tilde{f}^*(\hat{\tau}_n, \hat{\tau}) = \hat{\tau}_\xi^2 + \tilde{a}_2 \langle \hat{t}_n - t_{\xi n} \rangle - \tau_y^2 \tag{9}$$

To consider kinematic hardening a backstress vector t_ξ is introduced, which influences the position of the yieldcurve in the stress-strain domain due to plastic deformation.

$$\boldsymbol{t}_\xi = \begin{bmatrix} t_{\xi n} & \tau_{\xi t} & \tau_{\xi b} \end{bmatrix}^T = \begin{bmatrix} 0 & \tau_{\xi t} & \tau_{\xi b} \end{bmatrix}^T \tag{10}$$

After a change in the loading direction, the yield point is reduced by the amount of the backstresses. This phenomenon is also known as the BAUSCHINGER effect [11]. It is necessary to formulate the backstresses in terms of an effective value according to eq. 11.

$$\hat{\tau}_\xi = \sqrt{(\hat{\tau}_t - \hat{\tau}_{\xi t})^2 + (\hat{\tau}_b - \hat{\tau}_{\xi b})^2} \tag{11}$$

The equations, required for the numerical implementation, are chosen in rate form, following the authors ARMSTRONG and FREDERICK [12]. In this, b represents a saturation parameter and r is the plastic arc length.

$$\dot{\tau}_{\xi t} = E_{\xi t}\dot{\Delta}_t^{pl} - b|\dot{r}|\tau_{\xi t} \tag{12}$$

$$\dot{\tau}_{\xi b} = E_{\xi b}\dot{\Delta}_b^{pl} - b|\dot{r}|\tau_{\xi b} \tag{13}$$

$$\dot{t}_{\xi n} = E_{\xi n}\dot{\Delta}_n^{pl} - b|\dot{r}|t_{\xi n} = 0 \tag{14}$$

The description of the complete process requires the temperature and the state of cure dependent formulation of the plasticity equations. In this context, the isotropic hardening modulus, the initial yield stress as well as the kinematic hardening modulus are implemented as a function of the quantities mentioned, see eq. (15)-(17).

$$E_{\xi\theta}(\theta) = \frac{E_{\xi 0}}{2}\Big(1 + \tanh\big(m_\xi(\theta_\xi - \theta)\big)\Big) + E_{\xi 1} \tag{15}$$

$$\tau_\theta(\theta) = \frac{\tau_0}{2}\Big(1 + \tanh\big(m_\tau(\theta_\tau - \theta)\big)\Big) \tag{16}$$

$$H_\theta(\theta) = \frac{h_0}{2}\Big(1 + \tanh\big(m_h(\theta_h - \theta)\big)\Big) + h_1 \tag{17}$$

The state of cure dependent component is zero below the gel point and develops linearly after reaching it. This is represented by FÖPPL's bracket in eq. (18). The cure and temperature dependent kinematic hardening modulus in eq. (19) is defined as the product of χ_ξ and $E_{\xi\theta}$.

$$\chi_\xi(p) = \left\langle \frac{p - p_{gel}}{1 - p_{gel}} \right\rangle \tag{18}$$

$$E_\xi(\theta, p) = E_{\xi\theta}(\theta)\chi_\xi(p) \tag{19}$$

Parameter identification

The numerical model explained is adapted, based on thermal tensile tests of thick shear test specimens by varying the parameters and comparing them with the test data. For this purpose, the temperature-dependent parameters are first assumed to

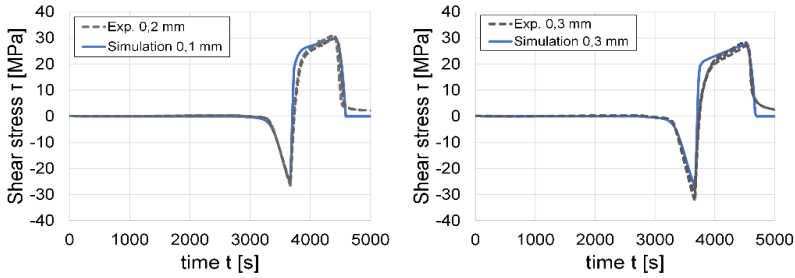

Figure 6: Numeric simulation of the process explained in the experimental section. Shear stresses are shown over time.

be constant and determined in a second identification step by curve fitting. The results of the identification process are shown in figure 6.
To describe the overall process, a kinematic damage is introduced which is not further explained here. This causes energy dissipation because of microcrack-induced released energy. Thus, after a load change, the full plastic strain hardening potential is not reached as it is in a steady process. Figure 7 shows the model's stress response to the displacement curves of the experimental thick shear test specimen as the simulation input.

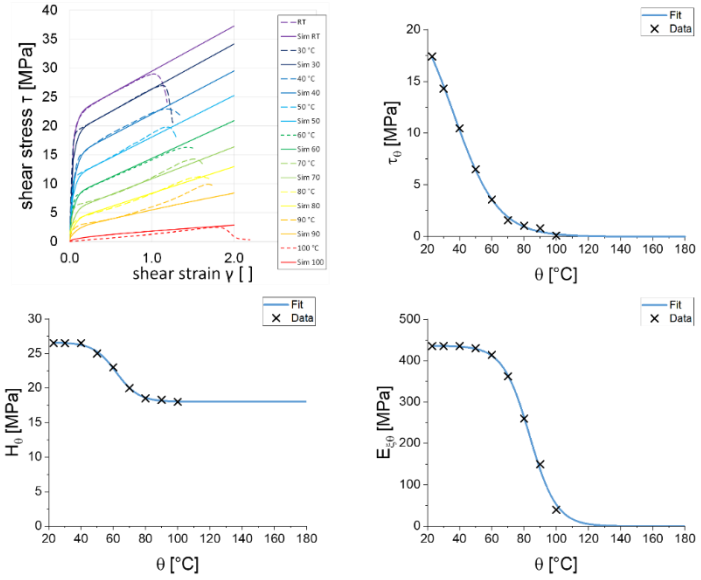

Figure 7: Result of the identification process of the temperature dependent material parameters. Experiments on a thick shear test specimen [13].

Conclusion

In conclusion, the mechanical properties of adhesive joints with relative displacements in the shear plane during curing show a great dependence on the magnitude as well as direction of the pre-deformation. Therefore, a non-time-reversible and anisotropic effect can be observed. The influence is still present under crash-like loading. For the numerical simulation model a phenomenological description of the material behaviour is achieved by the TAPO model extended to kinematic hardening and process-dependent damage. The transition from an isotropic to an anisotropic material behaviour as a result of manufacturing is illustrated. Additionally, the degree of hardening and temperature dependence are taken into consideration.
When pre-deformations in the normal direction occur, a reduction of the effective bonding area occurs. The subsequent property changes are primarily based on geometrical changes and not on the adhesive material itself.

Acknowledgements

All of the presented research results are part of IGF research project 20665 N by the Research Association for Steel Application (FOSTA), which was founded by the AiF under the Program for Promotion of Industrial Research (IGF) by the Federal Ministry for Economic Affairs and Climate Action (BMWK) based on a decision of the German Bundestag.

References

[1] M. Goede, M. Stehlin, L. Rafflenbeul, G. Kopp and E. Beeh, „Super Light Car—lightweight construction thanks to a multi-material design and function integration“, Eur. Transp. Res. Rev., Jg. 1, Nr. 1, p. 5–10, 2009, doi: 10.1007/s12544-008-0001-2.

[2] S. Menzel, „Zur Berechnung von Klebverbindungen hybrider Karosseriestrukturen beim Lacktrocknungsprozess“, Dissertation, Faculty of Mechanical Science and Engineering, Technische Universität Dresden, Dresden, 2011.

[3] DIN EN 14869-2:2011-07, Strukturklebstoffe_- Bestimmung des Scherverhaltens struktureller Klebungen_- Teil_2: Scherprüfung für dicke Fügeteile (ISO_11003-2:2001, modifiziert); Deutsche Fassung EN_14869-2:2011, Berlin, doi: 10.31030/1779680.

[4] DIN EN 15870:2009-08, Klebstoffe_- Bestimmung der Zugfestigkeit von Stumpfklebungen (ISO_6922:1987 modifiziert); Deutsche Fassung EN_15870:2009, Berlin, doi: 10.31030/1524436.

[5] F. Burbulla, A. Matzenmiller, Robustheit und Zuverlässigkeit der Berechnungsmethoden von Klebverbindungen mit hochfesten Stahlblechen unter Crashbedingungen. In: Research report P828, 2016.

[6] G. Meschut, A. Matzenmiller et al., Development of methods to simulate high strength adhesive joints with sheet steel at crash conditions for vehicle construction, In: Research report P676, FOSTA, Düsseldorf, 2008.

[7] S. Sourour und M. Kamal. „Differential scanning calorimetry of epoxy cure isothermal cure kinetics“. In: Thermochimica Acta 14.1-2 (1976), S. 41–59.

[8] G. Meschut, T. Aubel, A. Matzenmiller, P. Kühlmeyer, „Methodenentwicklung zur Simulation des thermomechanischen Verhaltens von Klebschichten und hybriden Fügeverbindungen während des Aushärteprozesses“, In: Research report P1087, FOSTA, Düsseldorf, 2018.

[9] P. Kühlmeyer, A. Matzenmiller, „Temperature dependent TAPO model for failure analysis of adhesively bonded joints due to temperature induced service loading“, 4. LS-DYNA Forum, 10.-12. October 2016, Bamberg, DYNAmore GmbH, Stuttgart.

[10] P. Kühlmeyer, A. Matzenmiller, „Constitutive modelling of thermo-viscoelastic-plastic behaviour of adhesively bonded joints“. Proc. Appl. Math. Mech. (PAMM), Vol. 14, Nr. 1, S. 325-326, 2014

[11] J. Bauschinger. „Über die Veränderung der Elastizitätsgrenze und der Festigkeit des Eisens und Stahls durch Strecken und Quetschen, durch Erwärmen und Abkühlen und durch oftmals wiederholte Beanspruchung“. In: Mitteilungen des mechanischtechnischen Laboratoriums der Königlich Technischen Hochschule München 13.1, 1886.

[12] P. J. Armstrong und C. O. Frederick. A mathematical representation of the multiaxial Bauschinger effect. Bd. 731. Central Electricity Generating Board [and] Berkeley Nuclear Laboratories, 1966.

[13] G. Meschut, D. Teutenberg et al., „Methodenentwicklung zur Simulation und Bewertung fertigungs- und betriebsbedingter Klebschichtschädigungen infolge Temperaturwechselbeanspruchung“, In: Research report P878, FOSTA, Düsseldorf, 2014.